SCIENTIFIC REPORTS

OPEN

SUBJECT AREAS:
CONDENSED MATTER PHYSICS
ELECTRONIC MATERIALS AND DEVICES
QUANTUM PHYSICS
SUPERCONDUCTING MATERIALS

Received
21 December 2011

Accepted
25 February 2012

Published
28 March 2012

Correspondence and requests for materials should be addressed to L.L. (lilu@aphy.iphy.ac.cn)

* These authors contributed equally to this work.

Strong Superconducting Proximity Effect in Pb-Bi_2Te_3 Hybrid Structures

Fanming Qu*, Fan Yang*, Jie Shen*, Yue Ding, Jun Chen, Zhongqing Ji, Guangtong Liu, Jie Fan, Xiunian Jing, Changli Yang & Li Lu

Daniel Chee Tsui Laboratory, Beijing National Laboratory for Condensed Matter Physics & Institute of Physics, Chinese Academy of Sciences, Beijing 100190, People's Republic of China.

To study the interface between a conventional superconductor and a topological insulator, we fabricated Pb-Bi_2Te_3-Pb lateral and sandwiched junctions, and performed electron transport measurements down to low temperatures. The results show that there is a strong superconducting proximity effect between Bi_2Te_3 and Pb, as that a supercurrent can be established along the thickness direction of the Bi_2Te_3 flakes (100~300 nm thick) at a temperature very close to the superconducting T_c of Pb. Moreover, a Josephson current can be established over several microns in the lateral direction between two Pb electrodes on the Bi_2Te_3 surface. We have further demonstrated that superconducting quantum interference devices can be constructed based on the proximity-effect-induced superconductivity. The critical current of the devices exhibits *s*-wave-like interference and Fraunhofer diffraction patterns. With improved designs, Josephson devices of this type would provide a test-bed for exploring novel phenomena such as Majorana fermions in the future.

Majarona fermions (MFs), novel particles which are their own anti-particles, were predicted more than seven decades ago but are yet to be identified[1]. Recently, much attention has been paid to search for MFs in condensed matter systems[2–10]. Among various proposed schemes, a typical one is to create MF at the interface between a conventional *s*-wave superconductor and a 3D topological insulator (TI)[11–13], where a proximity-induced state resembling a spinless p_x+ip_y superconductor is expected to occur. Experimentally, progresses have recently been made in the observations of a supercurrent over a relatively long distance in Nb-BiSb-Nb, Al-Bi_2Te_3-Al and W-Bi_2Se_3-W devices[14–16], a perfect Andreev reflection of the helical mode in InAs/GaSb quantum wells[17], and the opening of gap-like structures together with a conductance peak at the Fermi level in Sn-Bi_2Se_3 devices[18]. However, further characterizations are still needed to clarify the nature of the superconductor-topological insulator interface. In this work, we report the observation of a strong proximity effect in Pb-Bi_2Te_3 hybrid structures, based on which Josephson junctions and superconducting quantum interference devices (SQUIDs) can be constructed.

Results

Sample growth and device fabrication. Bi_2Te_3 single crystals were grown by Bridgeman method, and were confirmed to be of high quality by X-ray diffraction (Fig. 1a). The carriers are of electron type, with a concentration of $\sim 2\times10^{18}$ cm^{-3} as determined from the Hall effect and the Shubnikov–de Haas (SdH) oscillation measurements at 2 K (Fig. 1b). Thin flakes of Bi_2Te_3 with typical sizes of 10 μm in length/width and 100~300 nm in thickness were exfoliated from a bulk crystal and transferred onto Si/SiO_2 substrates. Pb electrodes of ~150 nm thick were fabricated onto the flakes via standard e-beam lithography, magnetron sputtering and lift-off techniques. To study the proximity effect along the lateral direction of the flakes, parallel Pb electrodes were directly deposited on top of the flakes (see insets of Figs. 2a and 2b). A more complicated sandwich structure (see Figs. 3a and 3b) was employed to study the penetration of the proximity effect in the thickness direction. The measurements were performed at low temperatures down to 15 mK in a dilution refrigerator or 250 mK in a ^{3}He cryostat. The differential resistance between two selected electrodes was measured as a function of both dc bias current and applied magnetic field with a quasi-four-probe measurement configuration. Precise control of magnetic field to milli-Gauss level is achieved by using a Keithley 2400 source meter to drive the superconducting magnet of the cryostat.

Proximity-effect-induced superconductivity in Pb-Bi_2Te_3-Pb lateral structures. To study the superconducting proximity effect along lateral direction, we have fabricated and investigated more than a dozen Josephson

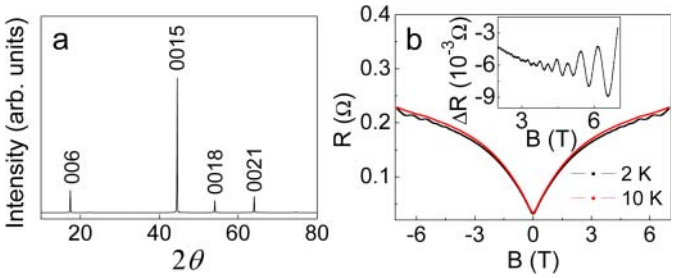

Figure 1 | Characterizations of the Bi_2Te_3 crystal used in this experiment. (a) X-ray diffraction pattern of the crystal. (b) Magneto-resistance of a Hall-bar shaped Bi_2Te_3 flake measured at 2 K (black) and 10 K (red) in perpendicular magnetic fields. The pronounced dip at zero magnetic field is caused by electron weak anti-localization due to strong spin-orbit coupling. Inset: difference of resistance between the 2 K curve and the 10 K curve, showing clearly the Shubnikov-de Haas oscillations at low temperatures, with an oscillation period of ~0.02 T^{-1}.

junctions that have parallel Pb electrodes of various lengths and inter-electrode distances deposited onto the top surface of the flakes. The insets of Figs. 2a and 2b show the scanning electron microscope (SEM) images of two types of junctions, one with Pb electrodes across the whole width of the flakes (junction #1, categorized as type-I), and the other with Pb electrodes located in the middle of the upper surface, away from the edges (junction #2, categorized as type-II).

Figures 2a and 2b show respectively the measured differential resistance dV/dI of the two junctions as functions of both magnetic field B and bias current I_{dc}. The dark blue region represents the zero-resistance superconducting state. It can be seen that the critical current I_c is modulated by magnetic field, demonstrating a Fraunhofer-like pattern as expected for an s-wave type Josephson junction[19]:

$$I_c(B) = I_c(0)\left|\sin\left(\frac{\pi\Phi_J}{\varphi_0}\right)/\left(\frac{\pi\Phi_J}{\varphi_0}\right)\right|$$

where $I_c(0)$ is the critical current of the junction at zero magnetic field, Φ_J is the flux through the junction area, and $\phi_0 = h/2e$ is the flux quanta.

The measured oscillation periods of the Fraunhofer pattern were consistent with the junction areas for all junctions. For example, the measured oscillation period for junction #2, $\Delta B = 1.45$ G, corresponds to an effective junction area: $S_{eff} = \phi_0/\Delta B = 14.3$ μm², which is consistent with the actual junction area $S = 13.8$ μm² estimated from the length (6 μm) and the center-to-center distance (2.3 μm) of the Pb electrodes (with the flux taken into account) .

For type-I junctions, the experimental data agree well with the theoretical Fraunhofer pattern (see, e.g., Fig. 2a for junction #1), with the ratio of the second peak height to the main peak height close to the expected value of 0.22. For type-II junctions, however, the measured oscillation patterns deviate significantly from the expectation,

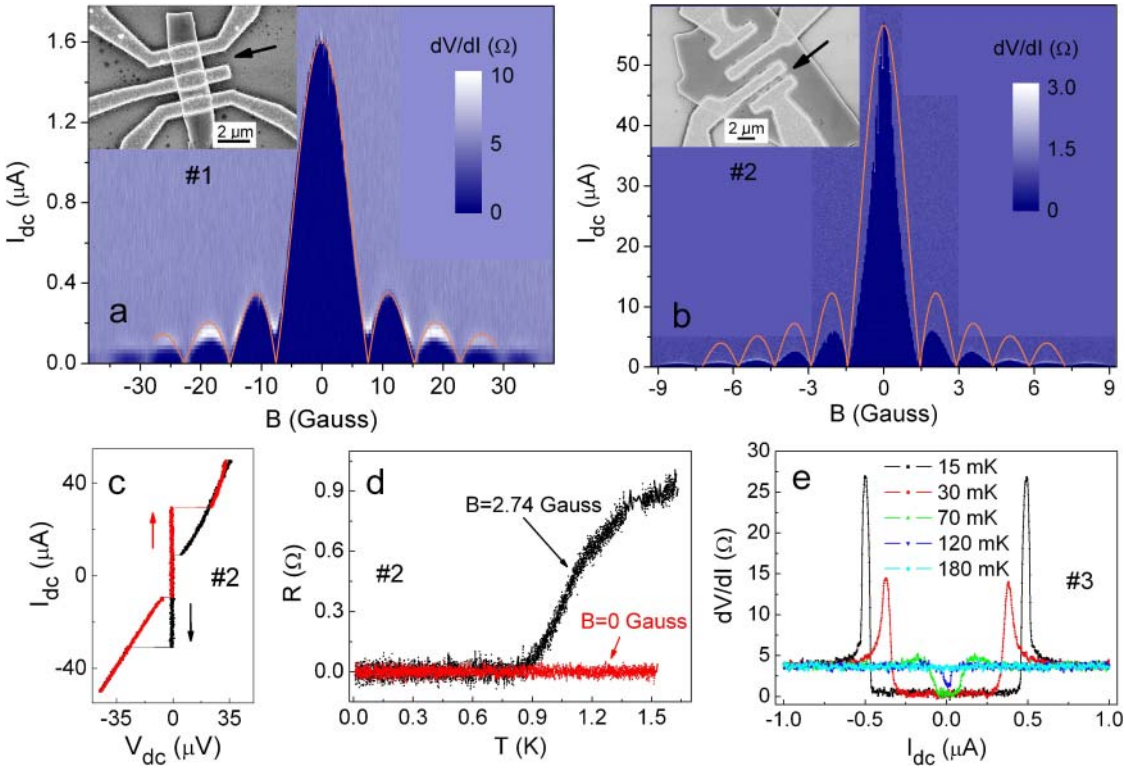

Figure 2 | Proximity-effect-induced superconductivity in Pb-Bi_2Te_3-Pb structures along lateral direction. (a) Inset: SEM image of type-I lateral Josephson junctions, with parallel Pb electrodes across the whole width of the Bi_2Te_3 flake. Main frame: a 2D image plot of the differential resistance dV/dI of junction #1 (indicated by the arrow), measured at 15 mK as a function of both magnetic field and dc bias current. The boundary of dV/dI from dark blue to light blue, which separates the superconducting state from the finite-resistance normal state, oscillates with magnetic field following the theoretically expected Fraunhofer pattern (the orange curve). (b) Inset: SEM image of type-II lateral Josephson junctions, with parallel Pb electrodes occupying the center part of the top surface. Main frame: The 2D image plot of dV/dI of junction #2 (indicated by the arrow), measured at 15 mK as a function of both magnetic field and dc bias current. The critical current oscillates with magnetic field in a way deviating from the standard Fraunhofer pattern. (c) I_{dc} *vs.* V_{dc} curve of junction #2 measured at 15 mK and in a magnetic field of 0.5 G, with bias current sweeping from positive to negative (black) and *vice versa* (red). Obvious hysteretic behavior can be seen. (d) Temperature dependencies of the zero-bias resistance of junction #2, measured in two different magnetic fields. (e) dV/dI *vs.* I_{dc} curves of junction #3 (type-I) composed of two Pb electrodes seperated by 3.5 μm, holding a supercurrent up to 120 mK.

with the peak height ratio ranging from 0.08 to 0.11 for seven such junctions investigated (the ratio is 0.1 for junction #2, see Fig. 2b). The results indicate a non-uniform spatial distribution of the supercurrent in type-II junctions[20], presumably due to the stray supercurrent flowing through the area near the two sides of the junctions.

Figure 2c shows one of the current vs. voltage (I_{dc} *vs.* V) curves of junction #2 at 15 mK. A hysteretic loop is seen in bi-directional current sweepings. We note that the asymmetric I_{dc}-V curve in uni-directional current sweeping is not likely to be caused by self-heating, because the hysteretic behavior remains in the junctions with a very small critical current (for example, junctions with a 1.5-μA critical current still exhibit obvious hysteretic loops see Fig. S1 of Supplementary information). Instead, the hysteretic behavior would indicate the formation of an underdamped Josephson junction[21] between adjacent Pb electrodes. An underdamped behavior is usually seen in planar tunneling junctions with significantly large junction capacitance and shunted resistance[19,21]. In our junctions, however, the capacitance should be negligibly small compared to planar tunneling junctions, and the junction resistance is only around one or several Ohms. Therefore, the appearance of a hysteretic behavior is quite unusual. It might be related to the strong spin-orbit coupling in Bi_2Te_3, being less dissipative because of reduced back scattering.

To examine how far a supercurrent can be established through proximity effect along the lateral direction, we have fabricated a number of junctions with different inter-electrode distances. For junction #2, which has an inter-electrode distance of 0.7 μm, a supercurrent held up to at least 1.5 K at zero magnetic field, as shown in Fig. 2d. For another junction with much longer inter-electrode distance of 3.5 μm (junction #3, SEM image not shown), a supercurrent held up to 120 mK, as shown in Fig. 2e. A 2D image plot of the differential resistance of junction #3 as a function of both magnetic field and bias current can be found in Fig. S2 of Supplementary information. The appearance of a proximity-effect-induced supercurrent over such a long distance would enable us to construct more complicated devices for testing various interesting physics.

Proximity-effect-induced superconductivity in Pb-Bi_2Te_3-Pb sandwich structures. To test whether a supercurrent can also be established via proximity effect along the thickness direction of the flakes, two sandwich-like devices were fabricated, and similar results were obtained. The device structure is shown in Fig. 3a and illustrated in Fig. 3b. A Pb film was firstly sputtered on one surface of the flakes when they were still on the Scotch tape after being exfoliated. Then those flakes of 100–300 nm in thickness were selected and transferred onto a Si/SiO_2 substrate, with the Pb side facing down to the substrate. Afterwards, an overexposed PMMA layer was coated to cover one side/edge of the selected flakes, serving as an insulating mask. Finally, two top Pb electrodes, with a same contacting area of ~3×2 μm^2 and separated by ~10 μm, were deposited on top of each flake. According to our previous investigation on lateral junctions, we know that no supercurrent can be established over ~10 μm distance along the lateral direction above 100 mK. Therefore, the measurement between the two top Pb electrodes actually probes the superconducting transition of the two sandwich junctions in the thickness direction.

Figure 3c shows the temperature dependence of quasi-four-probe resistance of device #4 between the two top electrodes. With decreasing temperature, the resistance of both devices undergoes two superconducting transitions around 7~8 K, one at a slightly higher temperature but with an obviously smaller resistance jump, the other at a lower temperature and with a larger resistance jump.

There are two possible scenarios for the occurrence of the two transitions. In the first scenario, the resistance jump at the higher temperature is caused by the superconducting transition of the bottom Pb film, which partially shorts out the flake, and the resistance jump at the lower temperature is due to the proximity-induced super-

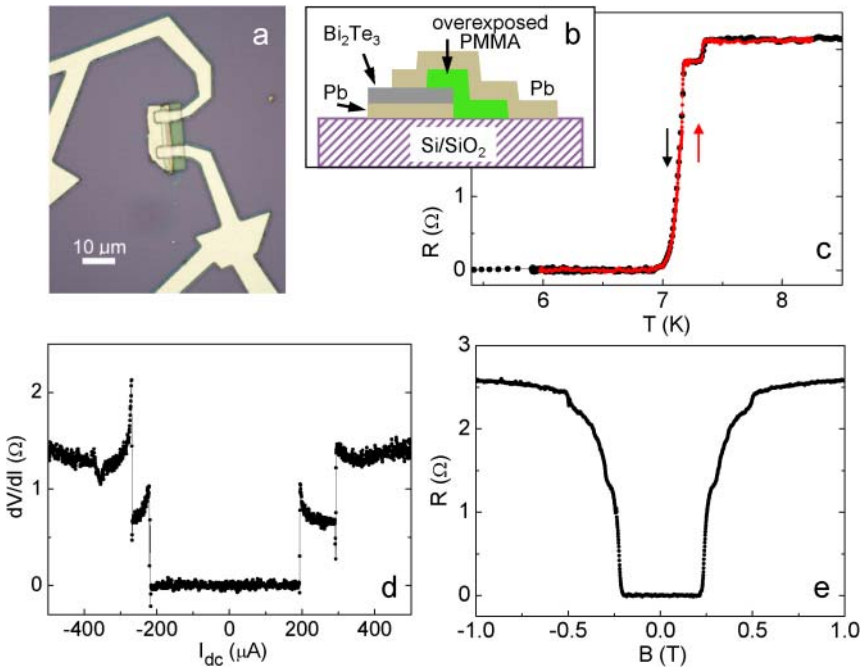

Figure 3 | Proximity-effect-induced superconductivity in Pb-Bi_2Te_3-Pb sandwich structures. (a) Optical image of a sandwich-structured device (device #4). (b) Illustration of the device structure. (c) Temperature dependence of the zero-bias resistance of device #4 measured from one top Pb electrode to another with a quasi-four-probe measurement configuration. Both ramping down (black) and up (red) curves are shown. The resistance jump at the higher temperature corresponds to the superconducting transition of the Pb film, and the jump at the lower temperature corresponds to the superconducting transitions of the two sandwich junctions occurred simultaneously. (d) A typical dV/dI *vs.* I_{dc} curve of device #4 measured at 0.3 K. The two jumps of dV/dI with similar amplitudes correspond respectively to the individual superconducting transition of the two sandwich junctions. (e) The magnetic field dependence of the resistance of device #4 measured at 0.3 K and with I_{dc}=0.

conducting transition of the two sandwich junctions. In the second scenario, these two resistance jumps correspond to the individual superconducting transitions of the two sandwich junctions, respectively.

The *dV/dI vs.* I_{dc} curve shown in Fig. 3d is in favor of the first scenario. As can be seen, two jumps with different critical currents appear on the *dV/dI vs.* I_{dc} curve. The two jumps there should all be ascribed to the superconducting transitions of the sandwich junctions, not that one to the superconducting transition of the junctions and one to the superconducting transition of the Pb film at the bottom, since the critical current of a Pb film should be much larger. The data in Fig. 3d tell us that the resistances of the two sandwich junctions are about the same before becoming superconducting. We therefore believe that the two resistance jumps in the *R vs. T* curve, with different but well-defined amplitudes (because of their step-like shapes), have different origins. We ascribe the jump occurred at the higher temperature to the superconducting transition of the Pb film, and the one at the lower temperature to the two sandwich junctions. Actually the lower transition of device #5 contains double jumps (see Fig. S3 in Supplementary information), which is likely due to a slight difference between the two sandwich junctions.

The onset transition temperature of the sandwich junctions is 7.17 K for device #4 and 7.15–7.2 K for device #5 (see Fig. S3 in Supplementary information), which is close to or only slightly lower than the superconducting temperature of bulk Pb (T_c=7.2 K). It indicates that a strong proximity effect occurs at the Pb-Bi_2Te_3 interface, which drives the flake in the whole thickness direction into superconducting state such a high temperature.

The T_c of the bottom Pb film is 7.34 K for device #4 and 7.8 K for device #5, which is higher than the T_c of pure Pb, indicating that an alloy phase is formed at the interface. The alloy phase is likely formed during the two baking processes, each at 180°C and lasting for 2 min, for making the over-exposed PMMA mask and the PMMA for defining the top Pb electrodes. If no baking process is applied after the deposition of Pb film on Bi_2Te_3, as in the preparation of our lateral Josephson junctions and SQUIDs, the onset T_c of the Pb film remains to be 7.2 K (see Fig. S5 in Supplementary information).

Construction of SQUIDs based on the proximity-effect-induced superconductivity. Based on the proximity-effect-induced superconductivity, more than ten SQUIDs with various shapes and areas were fabricated on the surface of Bi_2Te_3 flakes and measured down to dilution refrigerator temperatures. One of the typical results measured at 15 mK is shown in Fig. 4. The critical current of the SQUIDs shows standard interference patterns against magnetic field. In addition, the envelope of the interference pattern is modulated by the Fraunhofer diffraction patterns of each single junction. These behaviors can be described by the following formula[19]:

$$I_c(B) = 2I_c(0)\left|\sin\left(\frac{\pi\Phi_J}{\varphi_0}\right)/\left(\frac{\pi\Phi_J}{\varphi_0}\right)\right|\left|\cos\frac{\pi\Phi}{\varphi_0}\right|$$

where $I_c(0)$ is the critical current of each single junction at zero magnetic field, Φ_J is the flux through the single junction area, andΦ is the flux through the ring area of the SQUID.

The periods of both the interference and the Fraunhofer diffraction are found to be consistent with their corresponding areas, i.e., the areas of the ring and the junction, respectively. Specifically, from the data shown in Fig. 4, the observed periods are 0.48 G and 3.7 G, corresponding to areas of 43.2 μm^2 and 5.6 μm^2, which are in agreement with the measured areas of 38.5 μm^2 and 6.4 μm^2 for the ring and the junction, respectively. Since the effective areas of small SQUIDs are not easy to be determined if flux is being compressed by the surrounding superconducting electrodes, a SQUID with a large area and thinner arms were investigated. The result is shown in Fig. S4 of Supplementary information. It confirms that the period-to-area relation for conventional SQUIDs holds accurately in the Pb-Bi_2Te_3-Pb proximity-effect SQUIDs.

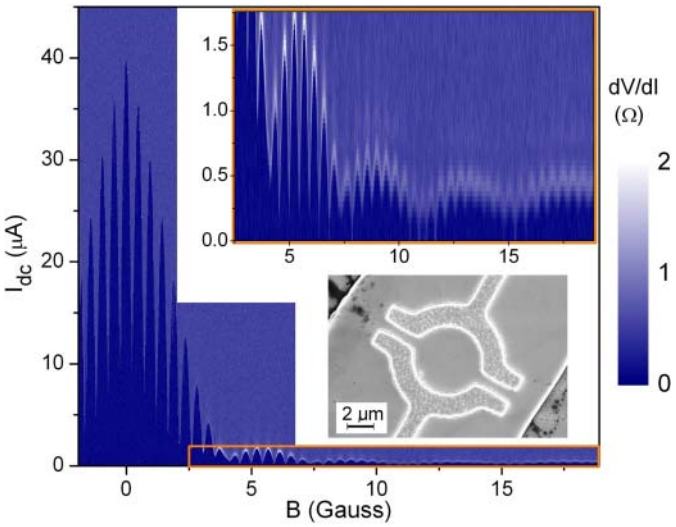

Figure 4 | Superconducting quantum interference device (SQUID) based on the proximity-effect-induced superconductivity. Lower inset: SEM image of a SQUID with Pb electrodes on the top surface of a Bi_2Te_3 flake. Main frame: differential resistance of the SQUID measured at 15 mK as a function of both magnetic field and bias current. Upper inset: Details of the orange rectangle region in the main frame, showing clearly the oscillations of critical current with magnetic field due to interference along the ring of the SQUID, and the modulation of the oscillations by the Fraunhofer diffraction pattern of the single junctions.

Discussion

We have demonstrated that a strong proximity effect occurs at the Pb-Bi_2Te_3 interface, i.e., the whole volume of Bi_2Te_3 flake beneath the Pb electrodes becomes superconducting at a temperature very close to the T_c of Pb electrodes, and that a Josephson supercurrent can be established over a distance of several microns between two Pb electrodes. To our knowledge, such a strong proximity effect is not commonly seen in literature. Its origin needs to be clarified. In particular, the Pb-Bi_2Te_3 interface needs to be characterized using crystallographic methods.

From the observed interference and Fraunhofer diffraction patterns, the maximum of critical current is located at zero magnetic field. It infers that the Josephson devices being investigated are of *s*-wave type. So far, no sign of unconventional pairing symmetry is recognized, presumably due to the dominating role of the Pb electrodes and/or the trivial superconducting feature of the Bi_2Te_3 bulk beneath the Pb electrodes. More sophisticated device structures are demanded to reveal the possible unconventional pairing symmetry at the *s*-wave superconductor/topological insulator interface, and to help searching for Majorana fermions at a device level.

Methods

Bi_2Te_3 single crystals were exfoliated to thin flakes using a Scotch tape. The flakes were then transferred onto Si/SiO_2 substrates. Top Pb electrodes on the flakes were fabricated by using standard e-beam lithography and magnetron sputtering techniques. For the sandwich-structured junctions, a layer of Pb film was firstly sputtered onto Bi_2Te_3 flakes while they have been exfoliated from a bulk crystal but still staying on the Scotch tape. Then the flakes were transferred onto Si/SiO_2 substrates with the Pb-side surface facing down, as confirmed by an optical microscope. An overexposed PMMA layer covering one edge of the flakes was then fabricated, serving as an insulating mask to prevent the top Pb electrodes from touching the bottom Pb film. During the fabrications of the over exposed PMMA mask layer and the top Pb electrodes, the bottom Pb-Bi_2Te_3 interface was baked twice at 180°C, each lasting for 2 min.

1. Wilczek, F. Majorana returns. *Nature Phys.* **5**, 614–618 (2009).
2. Fu, L. & Kane, C. L. Superconducting proximity effect and Majorana fermions at the surface of a topological insulator. *Phys. Rev. Lett.* **100**, 096407 (2008).

3. Qi, X.-L., Hughes, T. L. & Zhang, S.-C. Chiral topological superconductor from the quantum Hall state. *Phys. Rev. B* **82**, 184516 (2010).
4. Sau, J. D., Lutchyn, R. M., Tewari, S. & Sarma, S. D. Generic new platform for topological quantum computation using semiconductor heterostructures. *Phys. Rev. Lett.* **104**, 040502 (2010).
5. Sato, M., Takahashi, Y. & Fujimoto, S. Non-Abelian topological order in *s*-wave superfluids of ultracold fermionic atoms. *Phys. Rev. Lett.* **103**, 020401 (2009).
6. Fu, L. & Kane, C. L. Probing neutral Majorana fermion edge modes with charge transport. *Phys. Rev. Lett.* **102**, 216403 (2009).
7. Akhmerov, A. R., Nilsson, J. & Beenakker, C. W. J. Electrically detected interferometry of Majorana fermions in a topological insulator. *Phys. Rev. Lett.* **102**, 216404 (2009).
8. Seradjeh, B., Moore, J. E. & Franz, M. Exciton condensation and charge fractionalization in a topological insulator film. *Phys. Rev. Lett.* **103**, 066402 (2009).
9. Tanaka, Y., Yokoyama, T. & Nagaosa, N. Manipulation of the Majorana fermion, Andreev reflection, and Josephson current on topological insulators. *Phys. Rev. Lett.* **103**, 107002 (2009).
10. Law, K. T., Lee, P. A. & Ng, T. K. Majorana fermion induced resonant Andreev reflection. *Phys. Rev. Lett.* **103**, 237001 (2009).
11. Qi, X.-L. & Zhang, S.-C. The quantum spin Hall effect and topological insulators. *Phys. Today* **63**, 33–38 (2010).
12. Hasan, M. Z. & Kane, C. L. *Colloquium:* Topological insulators. *Rev. Mod. Phys.* **82**, 3045 (2010).
13. Moore, J. E. The birth of topological insulators. *Nature* **464**, 194–198 (2010).
14. Kasumov, A. Y. *et al.* Anomalous proximity effect in the Nb-BiSb-Nb junctions. *Phys. Rev. Lett.* **77**, 3029 (1996).
15. Sacépé, B. *et al.* Gate-tuned normal and superconducting transport at the surface of a topological insulator. *Nat. Commun.* **2**, 575 (2011).
16. Zhang, D. M. *et al.* Superconducting proximity effect and possible evidence for Pearl vortices in a candidate topological insulator. *Phys. Rev. B* **84**, 165120 (2011).
17. Knez, I., Du, R.-R. & Sullivan, G. Perfect Andreev reflection of helical edge modes in InAs/GaSb quantum wells. Preprint at http://arxiv.org/abs/1106.5819 (2011).
18. Yang, F. *et al.* Proximity effect at superconducting Sn-Bi_2Se_3 interface. *Phys. Rev. B* **85**, 104508 (2012).
19. Clarke, J. & Braginski, A. I. *The SQUID Handbook Vol. 1* (WILEY-VCH Verlag GmbH & Co. KGaA, Weinheim, 2004).
20. Dynes, R. C. & Fulton, T. A. Supercurrent density distribution in Josephson junctions. *Phys. Rev. B* **3**, 3015 (1971).
21. Heersche, H. B. *et al.* Bipolar supercurrent in graphene. *Nature* **446**, 56–59 (2007).

Acknowledgments

We would like to thank T. Xiang, L. Fu, G. H. Chen, Z. Fang and X. Dai for stimulative discussions. This work was supported by the National Basic Research Program of China from the MOST under the contract No. 2009CB929101 and 2011CB921702, by the Knowledge Innovation Project and the Instrument Developing Project of CAS, and by the NSFC under the contract No. 11174340 and 11174357.

Author contributions

L.L. and the first three authors F.Q., F.Y., and J.S. plannd the experiment. F.Q., F.Y., and J.S. carried out the experiment parallely. F.Q., C.Y and L.L. wrote the paper, and all authors discussed its contents.

Additional information

Supplementary information accompanies this paper at http://www.nature.com/scientificreports

Competing financial interests: The authors declare no competing financial interests.

How to cite this article: Qu, F. *et al.* Strong Superconducting Proximity Effect in Pb-Bi_2Te_3 Hybrid Structures. *Sci. Rep.* **2**, 339; DOI:10.1038/srep00339 (2012).